Testing and Comprehensive Modeling of a GIE Utilizing Atmospheric Propellants

IEPC-2013-354

Presented at the 33rd International Electric Propulsion Conference,
The George Washington University • Washington, D.C. • USA
October 6 – 10, 2013

D. Feili[1]
Astronautics Research Group, University of Southampton, SO17 1BJ, U.K.

B. Lotz[2], B. Meyer[3], H. Loeb
I. Physics Institute of Justus Liebig University, Giessen, D-35392, Germany

C. Collingwood[4],
TransMIT GmbH, D-35390 Giessen, Germany

H. Leiter, R. Kukies
Astrium GmbH BL Equipment and Propulsion, P.O. 1119, 74215 Möckmühl, Germany

M. Smirnova[5], S. Khartov,
Moscow Aviation Institute (National Research Center), Volokolamskoe Shosse 4, 125993 Moscow, Russia

and

D. Di Cara[6], A. Bulit[7]
ESA/ESTEC, Keplerlaan1, 2200 AG Noordwijk ZH, the Netherlands

Abstract: This paper presents the results of a test campaign on a radio frequency ion thruster running with atmospheric propellants O2 and N2. The results are used for a detailed plasma theoretical based modeling of the RIT thrusters running utilizing atmospheric propellants.

I. Introduction

EARTH observation is one of the most important application of the space technology for example for providing the temporal variations of the Earth's gravity field over a time span of several years with high spatial resolution (i.e. ~100 km, comparable to that provided by GOCE, while it is about ~500 km in GRACE) and higher temporal resolution than GRACE (which is limited to ~1 month interval between successive gravity field maps). Such a

[1] Senior Lecturer, Astronautics Research Group, University of Southampton, *d.feili@soton.ac.uk*.
[2] Physicist, University of Giessen, *benjamin.lotz@physik.uni-giessen.de*.
[3] Physicist, University of Giessen.
[4] Project Manager, TransMIT GmbH, *Collingwood@transmit.de*.
[5] PhD Student, Moscow Aviation Institute, *tdjemms@gmail.com*.
[6] European Space Agency, Electric Propulsion Engineer and EPL Test Manager, Directorate of Technical and Quality Management, Mechanical Department, Propulsion and Aerothermodynamics, TEC-MPE, *davina.maria.di.cara@esa.int*
[7] European Space Agency, Electric Propulsion Engineer and EPL Test Engineer, Directorate of Technical and Quality Management, Mechanical Department, Propulsion and Aerothermodynamics, TEC-MPE, *alexandra.bulit@esa.int*

mission will significantly improve our understanding on ice sheet and glaciers melting trends, continental water cycles, ocean masses dynamics, solid-earth deformations and other geophysical phenomena through the mass transportation (and the consequent temporal variations of the gravity field) produced within the Earth system. The
widely used weather satellites use detectors for electromagnetic waves for environmental monitoring, meteorology, map making etc. Most Earth observation satellites carry instruments that should be operated at a relatively low altitude, although the altitudes below 500-600 kilometers are in general avoided, because of the significant air-drag at such low altitudes. The idea of RAM-EP is using the gases in this height as propellant for a solar electric propulsion system for drag compensation1.

Figure 1. RIT10-EBB thruster running with N_2+O_2.

Under an ESA contract two types of electric thrusters were tested to show their ability to work with atmospheric gasses2. In the TransMIT GmbH at the University of Giessen a gridded ion thruster of RIT type was foreseen for this study. The thruster was based on the RIT-10 already flown on ARTEMIS. Figure 1 shows the RAM-RIT-10 EBB running with a mixture of N2 and O2. The thruster was being ran without any modifications in the main thruster parts like discharge chamber and extraction system. The RF generator was however to be modified to pass to the different plasma discharge in the thruster. The first tests with showed the ability of the thruster to work with N2 without a major problem. Using O2 as propellant showed however a strong degradation of the graphite made acceleration grid due to the chemical reactions between O2 and Graphite. Replacing the grid material showed a dramatic enhancement of the life time.

II. Experiment

A. Thruster

Test article is the ion thruster RIT-10-EBB /RAM-RIT-10, a Radio-Frequency-Ion-Thruster (RIT) which generates thrust by accelerating propellant ions in the electrostatic field of a grid system. The ions are generated in an alternating electro-magnetic field.

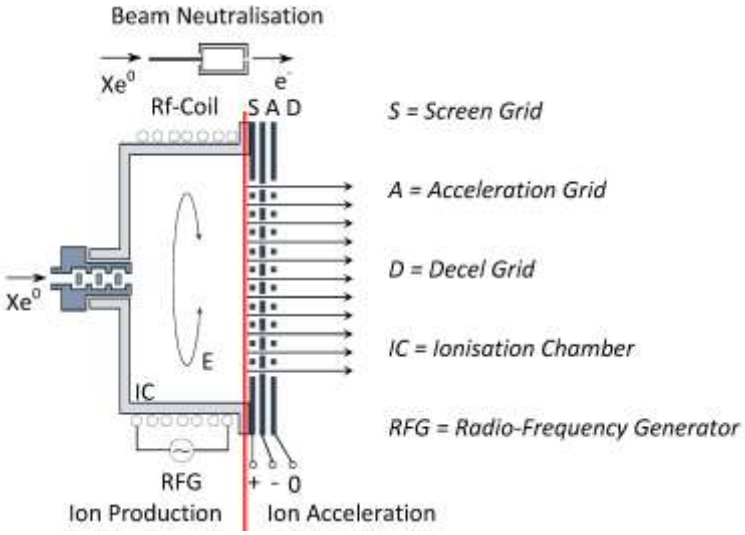

Figure 2: Scheme of an RF-Ion Thruster

Figure 3: View on grid-system

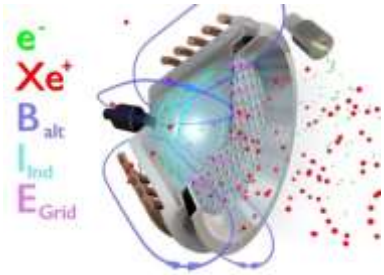

Figure 4: 3D-drawing by J. Mankiewicz

The propellant flow enters the ionizer via an isolator and a gas distributor. The ionizer vessel is made from an

insulating material and it is surrounded by the induction coil connected to rf-generator. The rf-generator is driving an AC current through the coil (**Fehler! Verweisquelle konnte nicht gefunden werden.**).
The axial magnetic field of the rf-coil induces an electrical eddy field, which accelerates the discharge electrons and enables them to ionize the Xe-atoms by inelastic collisions. Thus, an electrode-less, self-sustaining rf-gas discharge (plasma) is generated. By thermal movement the ions from the bulk plasma find the way towards the grid system. The rf-frequency is about 850-900 kHz. Finally the ions are accelerated in a system build-up of at least two grids. Concentric holes in these grids form a large number of single extraction channels. Every aperture of these channels is representing a single ion optical system. Their properties are determined by the diameters of the holes, the grid spacing and the applied voltages.

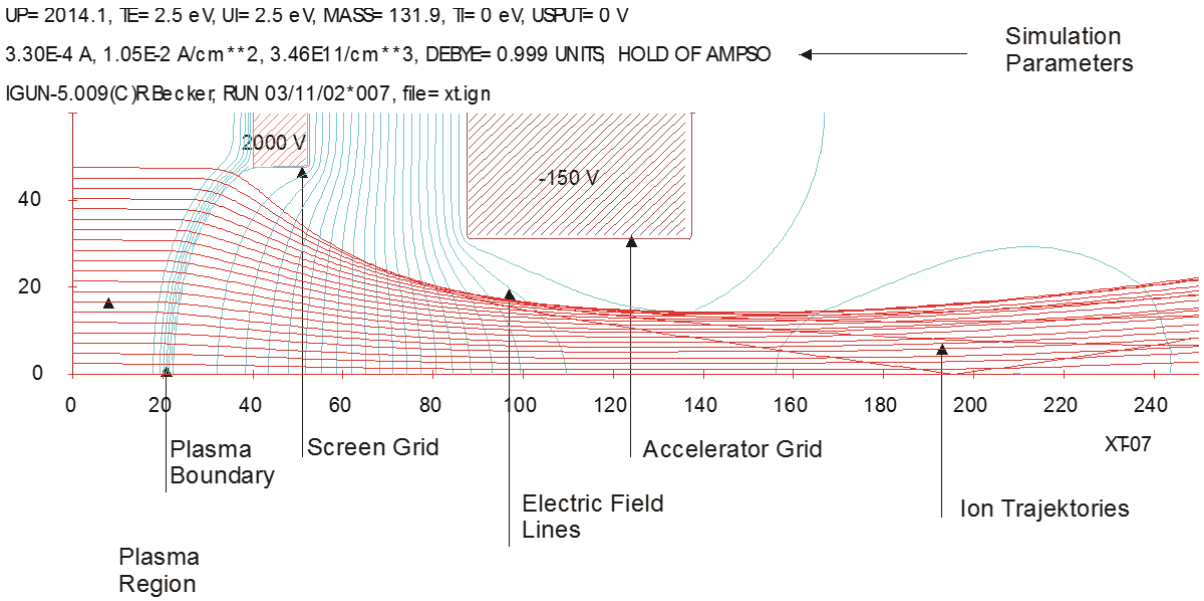

Figure 5: Simulation of one extraction aperture with Igun (simulated by R.Becker in 2002)

A positive voltage U_+ in respect to spacecraft ground is applied at the plasma sided screen grid and a negative voltage U_- at the second one. The negative voltage U_- at the "accelerator" grid prevents back-streaming of electrons from the downstream surroundings of the thruster into the ionization chamber and allows a higher voltage for ion extraction ($U_+ + |U_-|$) than for beam acceleration (U_+ only). Not all propellant atoms and or molecules leave the ionization chamber as ions, some remain neutral. The efflux of non-ionized atoms through the apertures of the grid system determines the propellant efficiency.
For the ignition of the radio frequency ion thruster it is necessary to insert free electrons to the discharge chamber. These electrons can gain energy through the rf-electric field to make an avalanche process to produce more electrons. The increase of the electron density stops when the discharge reaches the self-consistent state. The ignition of the RIT-10-EBB will be done using "pressure shock" as there will be no neutralizer used during this test campaign. In this method, the pressure in the thruster will be increased very fast to very high pressures. This, in combination with rf-power and (if necessary) high voltage, results in an increase in electron density which will be used for ignition. For the flight hardware this will be done by switching the polarity of the accel-grid to pull the electrons from the neutralizer to the discharge chamber. After the ignition the polarity of the accel-grid will be set to NHV again.
The RIT-10 is an ion engine with a 10 cm in diameter ionizer and a classic three grid system. The thruster is optimized for a thrust level of 15 mN (Xenon).
The RAM-RIT-10-EBB thruster has the same thruster parameters as the RIT-10 ARTEMIS. The ion optics and the discharge chamber as well as the radio frequency design parameters like inductivity and impedance are the same. The grid system and the interface between the discharge chamber and the extraction system were designed for the maximum flexibility and to simplify changing the parts.
The extraction system is made up of three grids as for the RIT-10 ARTEMIS. The grid system parameters like distance between the grids, grid thicknesses, and aperture or hole diameters are all kept unchanged.

For the tests with N_2+O_2 mixtures the thruster is equipped with an acceleration grid made up of Titanium instead of graphite, which showed an excessive corrosion due to the chemical interaction with O_2. The Titanium grid has the same geometry parameters as the Graphite grid. The ion optics and the thickness are the same.
In comparison to the flight hardware, besides the water cooling, the thruster is heavier and cannot stand a vibration test. It is however much more flexible and the changes in the discharge chamber, radio frequency design (coil design, thruster internally installed capacitors) and extraction system can be performed very easily if required.
Besides the changing in the extraction system of the RIT-10-EBB, there was another modification done on the thruster/rf-generator. During the tests of the thruster with N_2 and O_2 in the section one and two of the activity, it was seen, that the thruster had very low impedance. It caused a limitation of the maximum rf-power, which could be matched to the thruster, as the rf-generator can work up to a specific current. A new rf-design was performed and an impedance transformation was carried out by installing some capacitors inside the rf-generator and inside the thruster. This resulted in lower currents in the coil but higher voltages. The optimized version of the RIT-10-EBB is named as RAM-RIT-10.

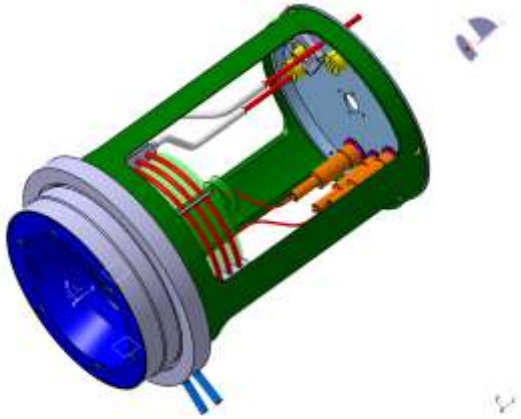

Figure 6: CAD-drawing of the RIT-10-EBB

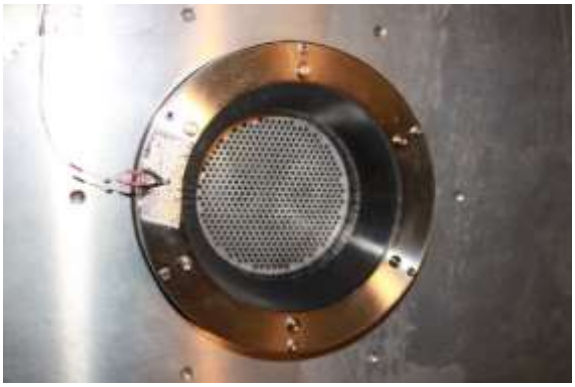

Figure 7: Mounted RIT-10-EBB frontal view

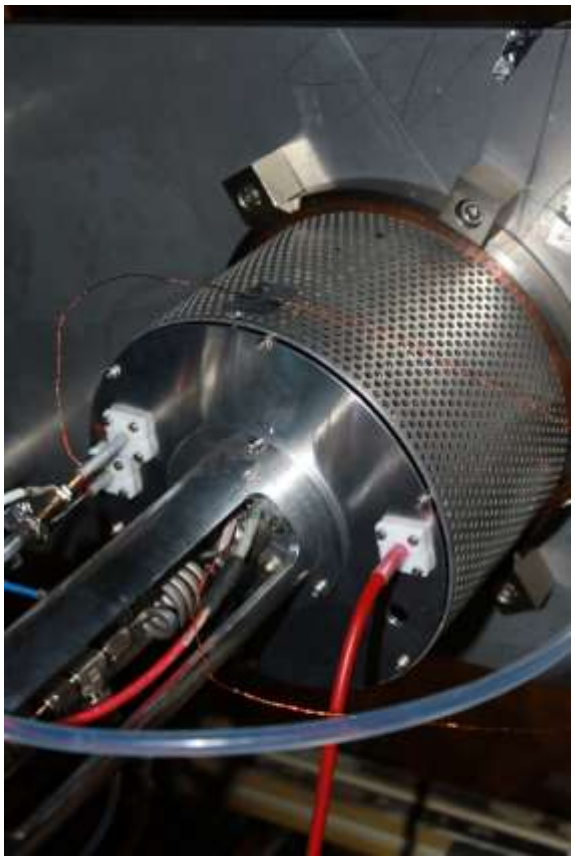

Figure 8: Mounted RIT-10-EBB from backside

B. Experimental setup

The test setup used for the entire test consisted of the test power supply of EADS, two different flow panels; the EADS thrust balance and the RAM-EP-10 Thruster. The Jumbo vacuum test facility has provided the environmental vacuum condition to operate the thruster. For the first and the second test session (N_2 and O_2 Test campaign) the flow panel from EADS was used. After the completion of these tests the flow panel was replaced by the new developed gas mixing panel. The total layout of the FCU and PSCU (TPS4) used during the whole test campaign is summarized in the following figures and described in more detail in the next chapters. The thrust balance could only be used in the first two test campaigns due to the limitations of the construction work of the new chemistry building directly next to the lab. The vibrational and oscillating loads created by the building machines prevent a possible and reliable measurement during the mixture test campaign. Several tries to measure a realistic value were not successful. Also the complete balance setup was misaligned by these loads; even in the night and without the daily

noises the measured results were not acceptable and realistic. Therefore the thrust was only computed for this mixture test campaign.

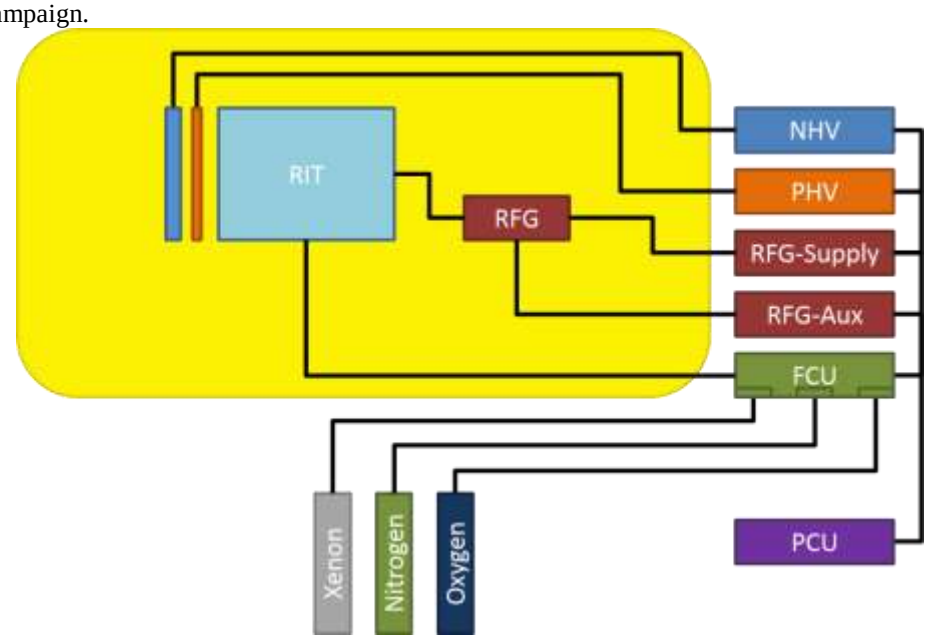

Figure 9: Overview of the schematically electrical setup

C. Results

The thruster performance was measured by changing the RF power, voltage and the gas flow. The maximum thrust reached with this thruster was 17.44mN by a total power consumption of 1.24kW and a gas flow of 0.3 mg/sec. figures 10 and 11 show the performance mapping of the thruster using Nitrogen and Oxygen respectively, always with Xe performance for comparison.

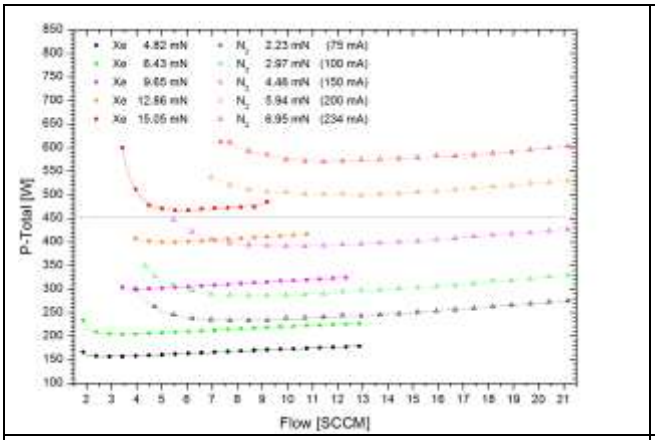

Figure 10: Performance comparison between Xe and N_2

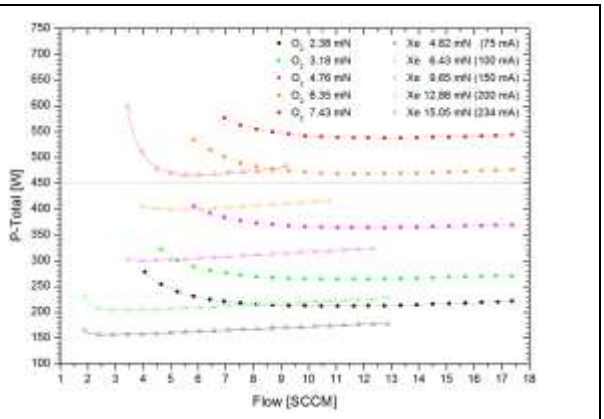

Figure 11: RAM-EP-10 thruster performance curves for O_2 and Xe with respect to the total power

III. Theory

This chapter summarizes the fundamental processes of a radio frequency ion thruster and the required diagnostics. The RIT-technology is based on an electrode-less discharge. An alternating electromagnetic field accelerates

electrons inside the discharge chamber on circular paths. Once they have gathered enough energy the electrons can react in different ways with their environment.

D. Modeling inputs

To establish a mathematical model of RIT-engines running with atmospheric gases, four fields of former and recent investigations might be used (see Figure).

1st **Discharge theory:** The extractable ion beam current I_i depends on the gas pressure p_i or the neutral gas density n_0 in the ionizer, on the electron temperature T_e and the electron or plasma density n_e, as well as on the propellant species, e.g. on the ionization cross section q_i

2nd **Discharge performance:** The dependency of the extracted ion current I_i on the rf-power P_{rf} and the gas flow rate $\dot{V}$ is to be measured in the frames of this thesis directly with a 10 cm rf-ion thruster for Xenon and atmospheric gasses O_2 and N_2.

3rd: **Extraction performance and theory:** Whether the beam current I_i offered by the plasma could really be extracted by the grid system, depends not only on the plasma data, but also on the extraction voltage U_{ex}, the grid geometry, and the propellant species.

4th **Discharge diagnostics:** By means of movable triple Langmuir probes, the plasma data T_e and n_e are to be measured as functions of the incoupled rf-power P_{rf} and the discharge pressure p_i. The ion beam yield I_i of the plasma can be calculated by $n_e\sqrt{T_e}$ (see F).

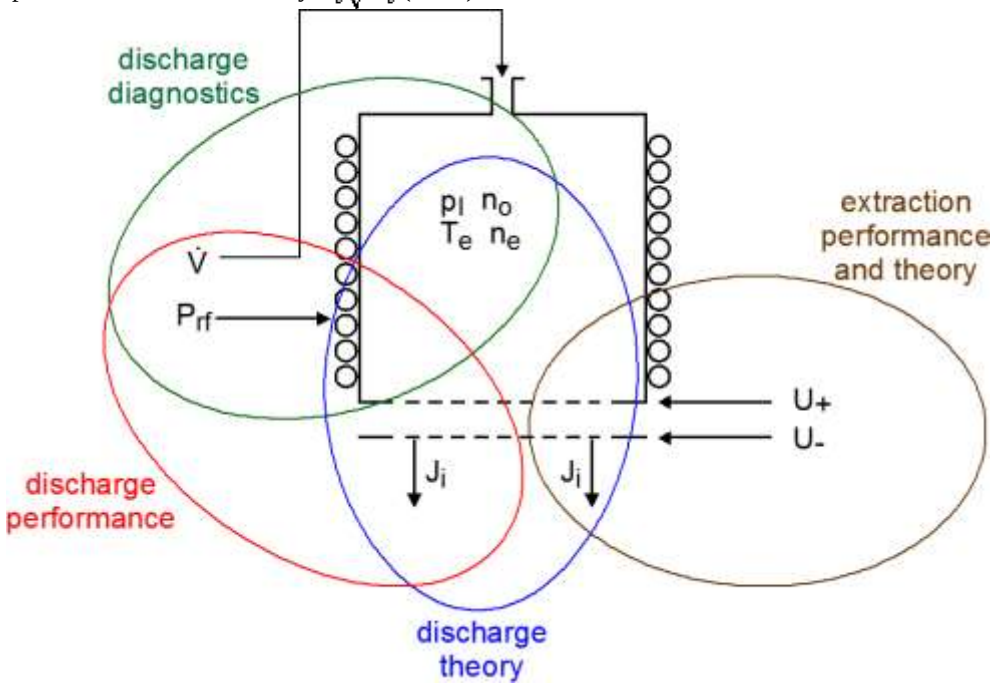

Figure 12: Four theoretical or experimental fields of investigation applied to establish a RIT-10 thruster performance model for operation with atmospheric gases

E. RF-Ionization

The propellant (Xe, N_2, O_2, etc.) of an rf-ion thruster of the RIT-type is ionized by an electrode-less radio-frequency gas discharge. For this purpose, the induction coil of an rf-generator (RFG) surrounds the ionizer vessel made of a dielectric material. The coil generates an approximately axial rf-magnetic field which induces an electrical eddy field E_{ind} of the same RFG-frequency. Discharge electrons, have been generated in previous ionization collisions, are accelerated in this field. They gather energy until they are able to perform ionizing processes themselves.
Besides the ignition case, the self-sustaining discharge does not need a discharge cathode for a permanent electron supply. The induced annular electric field strength is given by

$$E_{ind} = \frac{\mu_0 N_c}{2 l_c} \gamma_c r \omega \cdot I_{co} \cos \omega t \qquad 1$$

Herewith μ_o means the magnetic field constant, N_c the number of coil windings, l_c the coil length, γ_c a correction factor for short coils, r the distance from the axis, ω the angular frequency and I_{co} the amplitude of the coil current.
As E_{ind} is normally not high enough that an electron at rest can gather the necessary ionization energy during half of an rf-period (after which the direction of E_{ind} turns), an energy accumulation process must take place. Acceleration phases and elastic collisions with neutral gas particles take place alternatively resulting in a back and forth movement of the electrons. As this process follows the statistics, the electrons in an rf-discharge assume a Maxwell-Boltzmann distribution characterized by an electron temperature T_e. To enhance this energy accumulation process, the discharge pressure p_I should be adapted to the rf angular frequency ω. Both depend not only on the propellant species (mean free path) but also on the ionizer radius R (scaling laws see (9)):

$$p_I \sim \omega \sim \frac{1}{R} \qquad 2$$

The collision statistics with a Maxwellian distribution dn/n of the ionizing electrons, integrated over all electron energies W_e, yields the number of ionization collisions N_I per volume V and time t (10):

$$\frac{\partial^2 N_I}{\partial V \partial t} = \sqrt{\frac{8}{2\pi m_e}} \cdot n_0 n_e \cdot (kT_e)^{-3/2} \cdot \int_0^\infty q_i(W_e)\, W_e \cdot e^{-W_e/kT_e} dW_e \qquad 3$$

Figure shows (for Xenon) the ionization integral factor $f_I = \frac{dn}{n} \cdot q_i \cdot W_e$ together with the Maxwellian-distribution dn/n of the electrons and the ionization cross section q_i. This integral $\int f_I dW_e$ (together with the densities of the neutrals n_o and electrons n_e) is proportional to the ionization rate $\partial^2 N_I / \partial V \partial t$.
Figure compares f_I of O_2 and N_2 with Xe. Note that as a consequence of the lower q_i data, the ionization integral factors of O_2 and N_2 are by the factor of 10 smaller (see figure 14).

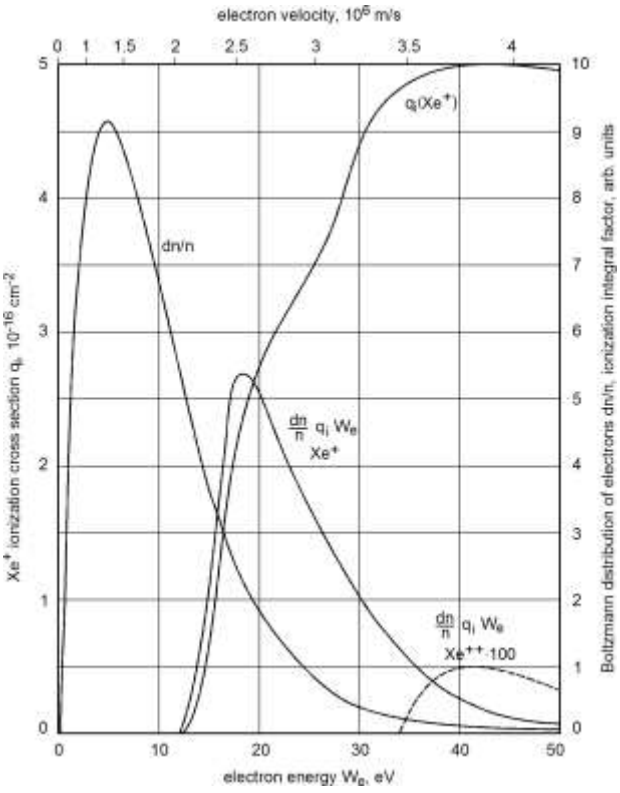

Figure 13: Maxwell-Boltzmann distribution dn/n of electrons with a maximum at 5 eV, ionization cross section q_i of $Xe^+$and ionization integral factor $f_I = dn/n \cdot q_i \cdot W_e$ vs. the electron energy W_e note that 18 eV-electrons ionize the best; the dashed f_I-curve of the Xe^{++} shows the small percentage of double charged ions in an rf-thruster

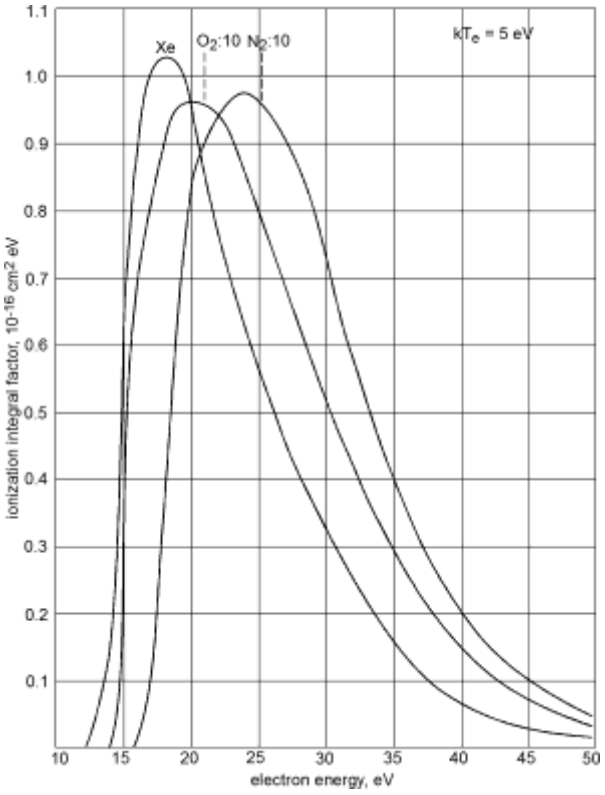

Figure 14: Calculated ionization integral factor $f_I = dn/n \cdot q_i \cdot W_e$ of Xe, O_2 and N_2 vs. the electron energy W_e; the O_2 and N_2 curves are enlarged by a factor of 10

F. Plasma balance and yield

In the equilibrium, the number of generated ions and electrons (see above) must be equal to the number of carrier losses by recombination and by the extraction through the grid system (see below).

In a low-pressure discharge, i.e. in the plasma of a RIT-10 engine, ion-electron recombination takes place mainly at the walls.

To guarantee that the same number of ions and electrons reaches the (isolating) ionizer walls, a plasma-wall potential V_P is built up automatically, that accelerates the heavy ions and decelerates the very mobile electrons, i.e. repels all electrons of the Maxwellian distribution having less energy than eV_P. The plasma-to-wall current is called ambipolar current.

The plasma potential (being positive with respect to the wall) amounts to:

$$V_P = \frac{kT_e}{2e} \cdot \ln\left(\frac{m_i}{2\pi m_e}\right) \qquad 4$$

Whereas m_i is the ion mass and $m_e$the electron mass. The logarithmic factor is for Xenon 10.55, for Oxygen 9.14 and for Nitrogen 9.01. Assuming an electron temperature of 5 eV, which is a good approximation for the RIT-10 as described above, the plasma potential in a Xe-discharge is about 26 V. Counting with $kT_e \geq 10\ eV$ for O_2 and N_2

(see above), the potential V_P would in both cases exceed 45 V. The rf-power consumption of the plasma is required for the ionization, the ambipolar current losses and for dissociation and excitation processes.
The ionization power losses (10) are given by the ionization rate and the energy of the ionizing electrons W_e (see Figure 13) integrated over the discharge vessel volume V_I:

$$P_I = \int \frac{\partial^2 N_I}{\partial V \partial t} \cdot W_e dV \qquad 5$$

The ambipolar losses $P_A$depend on the ambipolar current density j_A, the plasma potential $V_P$and the surface of the ionizer walls A_I (without the extraction part) (14):

$$P_A = \int j_A V_P dA_I \qquad 6$$

With $j_A = q_{ion} n_i v_i$ and $v_i = \sqrt{2 q_{ion} V_P / m_i}$ one may write:

$$P_A = \sqrt{\frac{2}{m_i}} \left(q_{ion} V_P\right)^{-3/2} \cdot \int n_i dA_I \qquad 7$$

Hereby, $q_{ion} = 1.01\ e$ stands for the mean ion charge (at 1 % of doubly charged ions) (15); m_i means the mean ion mass (molecular and atomic ions), and $n_i = n_e = n$ is the plasma density.
Note that the plasma density decreases towards the walls due to the ambipolar current.
The power losses by dissociation of the N_2 and O_2 molecules and by excitation collisions may be calculated by Equ. 7 too, provided that the related cross sections will be used for the dissociation and excitation rate.
Note that the very high dissociation energy of 9.79 eV for $N_2 \rightarrow 2N$ and the very low cross-section of the dissociative ionization $N_2 \rightarrow N^+ + N$ suggest to neglect any dissociations of N_2; however, this statement is not valid for O_2 ($W_{diss} = 5.15\ eV$).
As there exist several excitation levels (including rotation-vibrations), it is very difficult to calculate the excitation losses in the plasma.
In addition, non-plasma rf-power losses appear in a RIT-engine such as eddy currents in metallic thruster parts (e.g. in the screen grid) and dielectric losses in the isolating discharge vessel, both depending on the frequency and on material properties.
Therefore, it is practical to introduce the ion production costs w_i (given in eV/ion) that summarize all the named rf-power losses $P_{rf} = P_I + P_A + P_{diss} + \ldots$ necessary to generate one beam ion:

$$w_i = P_{rf} / I_i \qquad 8$$

This quality factor w_i, which will be used for RAM-EP modeling, depends mainly on the propellant species, the discharge frequency, the discharge pressure, and the thruster size.
Note that the extracted ion beam I_i depends on the extraction area A_{ex} of the first grid only, whereas P_I, P_A etc. depend on the volume V, or the wall surface A of the total ionizer, respectively. This fact suggests optimizing the discharge vessel length as well as the ionizer shape (cylindrical, semispherical, elliptical, etc.).
As a plasma-boundary transition sheath is built up in front of the extraction system in which the plasma ions are pre-accelerated and the electrons are decelerated, we get the extractable, i.e. by the plasma yield limited beam current:

$$I_i = 0.6065 \cdot q_{ion} \cdot n_i \cdot \sqrt{\frac{kT_e}{m_i}} \cdot A_{ex} \quad with \quad A_{ex} = N \pi r_1^2 \qquad 9$$

Hereby N is the number of beamlets and r_1 the radius of the borings in the first grid.
Note that this plasma-saturation current cannot be calculated by the macroscopic operational parameters, i.e. the rf-power P_{rf} and the propellant flow rate $\dot{V}$. The microscopic plasma parameters n_i and T_e must be measured by a

plasma diagnostic method. For a known or given beam current and a gas density n_o the plasma parameters could be calculated. For it the equation 3 (with $I_i = q_i dN_i/dt$) has to be equalized with the equation 9, taking V_I/A_{ex} into account.

As the result, the mean electron temperature T_e in a N_2 and O_2 discharge is 10 to 13 eV ($T_e(Xe) = 5\ eV$), whereas the mean plasma density n_e amounts to about $0.8 \cdot 10^{11}/cm^3$ ($n_e(Xe) = 3 \cdot 10^{11}/cm^3$). Following Equ.4, the plasma potential V_P in N_2 and O_2 discharges is 45 to 60 V ($V_P(Xe) = 25\ V$).

G. Discharge characteristics

The performance mapping of the discharge yields the basic discharge curves $I_i(P_{rf}, \dot{V})$. The curves give the rf-power P_{rf} vs. the gas flow rate $\dot{V}$ needed to produce a beam current I_i as the parameter (provided that the grid system is able to extract the total plasma yield).

The curves show that the required rf-power could be throttled if the gas flow is increased and vice versa.

The analysis shows that the curves have a (nearly) hyperbolic shape:

$$I_i \approx a \cdot \left(P_{rf} - w_o \cdot I_i\right) \cdot \left(\dot{V} - g_o \cdot I_i\right) \qquad 10$$

(In the case of the former N_2 measurement, the P_{rf}-requirements increase somewhat again at high propellant flow rates which may be caused by increasing elastic collisions.)

The hyperbolic parameter a (given in $mA/W \cdot SCCM$) (11) increases strongly with the ion mass and affects the shape of the curves (which have in the case of Hg nearly a L-shape, note that Hg was used in the past as a propellant, but was replaced by Xe).

The horizontal asymptote $w_o \cdot I_i$ (with w_o in eV/ion) stands for all rf-power losses outside the plasma.

The vertical asymptote $g_o \cdot I_i$ gives the gas flow of the extracted ions only with $g_o = 13.93\ SCCM/A$ for all propellants.

If there are no other constraints (e.g. a limited power budget of a satellite), the optimum operational point (with the maximum overall efficiency of the thruster) is found at the bending points of the I_i-curves. When throttling the engine, the working line should cross the different bending points.

The discharge characteristics $I_i\left(P_{rf}, \dot{V}\right)$ give the main input for a RIT modeling.

H. Ion extraction and beam formation

The plasma ions are extracted out of the ionizer, accelerated, and focused to beamlets by three multi-hole electrodes namely the screen grid, the accel grid, and the decel grid or a decel ring.

- **The screen grid** is biased on positive high voltage U_+ and it fixes the plasma potential which assumes at thrusting $U_+ + V_P$ versus ground. Thus, the power output of the positive high voltage generator (PHV) should be $I_i \cdot U_+$, whereas the beam power would be $I_b\ (U_+ + V_P)$. Note that $I_b V_P$ is a contribution of the rf-generator. The beam current I_b is defined as the extracted ion current I_i minus the drain current I_{acc} on the accel grid.

  As been mentioned already, all ions entering the apertures of the screen grid are subjected to the electrostatic fields in the grid system. As this region is free of electrons, one can observe a positive space charge. To keep the discharge plasma quasi-neutral, an electron current, being equal to I_i, must be collected by the interspaces between the extraction holes of the screen grid.

- **The accelerator grid** is biased on negative high voltage U_- (NHV). Thus, the extraction voltage U_{ex} is given by U_+ plus the absolute value of U_-. Besides an extraction improvement, the negative accel grid stops also back-streaming electrons. The NHV power requirement amounts to $I_{acc} \cdot U_-$. The drain current I_{acc} originates mainly from ion charge exchange processes (CEX) in the grid system. The slow CEX-ions may be attracted by the negative accel grid and sputter it by impact. This effect causes the lifetime limitation of the engine.

- **The decelerator grid** or decel ring is grounded, decelerates the beamlet ions down to the original energy of $q_i(U_+ + V_P)$, and protects the accel grid against back-streaming ions from the thruster exit or neighborhood (CEX-ions, neutralizer ions).

  If the extraction voltage U_{ex} is well adapted to the plasma yield, then the transition sheath, the plasma boundary and the upper equipotential planes are vaulted in a concave way (see Figure III-1). This works as an ion-optical immersion lens and focuses the ions. In the optimum focusing case, the focal length should be equal to the accel length d. Then, the focal spot is found inside the accel grid borings, which consequently can be made smaller than the screen grid holes to save neutral gas losses (see below).

Note that the defocusing effect in the downstream, deceleration part of the grid system is less effective than the focusing effect due to the increased stiffness of the beamlets.
In the so-called over- or under-focused case, U_{ex} is either too high or too low. The plasma boundary vaults too much or not much enough into the plasma and the focal length is either too short or too long, respectively. In both cases, the accel drain current I_{acc} increases.

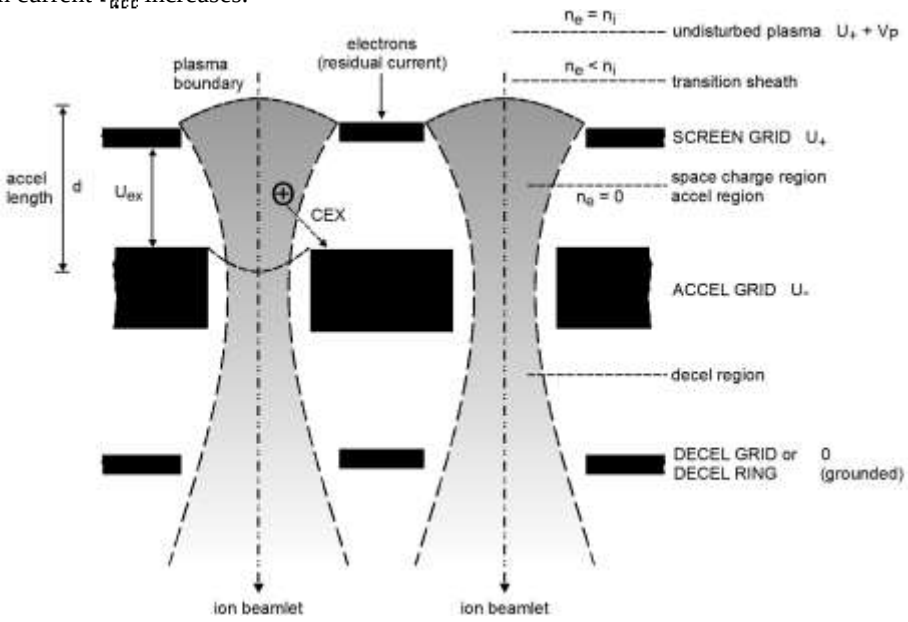

Figure III-1: Sketch of the grid system of a RIT-engine with two exemplary beamlets (11).

Due to the space charge in the accel region, the extractable ion current I_i is limited by Langmuir-Schottky-Child's law (ε_0 = electric field constant) (18):

$$I_i = \frac{4}{9}\varepsilon_0 \cdot \sqrt{\frac{2q_{ion}}{m_i}} \cdot \frac{U_{ex}^{3/2}}{d^2} \cdot A_{ex} \qquad 11$$

The designer of a grid system and the operator of an rf-engine must care for two conditions:

1st The ion current limited by the plasma yield should at least be equal to the space-charge limited current (depending on U_{ex} and d). That means that all ions, offered by the plasma, should really be extracted, whereas too high extraction voltages don't enhance the beam current, but instead causes beamlet over-focusing and break downs between the grids as well.

2nd The grid geometry (grid thicknesses, boring diameters and interspaces) should be designed in such a way that for the envisaged working parameters ($\dot{V}$, P_{rf} and U_{ex}) the optimized focusing is maintained.

The ion current density $j_i = I_i/A_{ex}$ delivered by the rf-plasma has a rather flat profile across the extraction area. This is caused by the relation $j_i \sim n_i\sqrt{T_e}$, since the electron temperature T_e increases and the plasma density $n_e = n_i$

decreases near the ionizer periphery. This flat $j_i(r)$ profile enables to keep the grid geometry unchanged across the total extraction system.
The optimum grid geometry depends not only on the desired beam voltage and the ion current density, but also on the propellant species. Transforming the Equation 11, one gets:

$$d \sim m_i^{-1/4} \cdot j_i^{-1/2} \cdot U_{ex}^{3/4} \qquad 12$$

It is clear, that not only the acceleration distance d but all geometrical data must be changed according to Equ. 11 and 12 with respect to the standard geometry of the RIT-2.5, RIT-15, and RIT-22. In the case of the variation of the beam voltage, this rather simple scaling law has been proved already by ion trajectory simulation (IGUN-computer program).
Thus, changing the propellant from Xe to O_2 or N_2 and keeping j_i and U_{ex} constant, the geometric values (grid thicknesses, extraction hole-diameters and interspaces) should be enlarged by a factor of 1.42 and 1.47, respectively according to Equ. 12 and using the masses of Xenon, Nitrogen and Oxygen. E.g., operating the thruster with an O_2/N_2 mixture, the screen grid holes should have diameters of 2.75 mm (for $j_i = 11.8\ mA/cm^2$ as RIT-22 with $175\ mN$). Naturally, the number of beamlets N should be reduced corresponding to $N \sim 1/d^2$ if the thruster size and the open area are kept constant.

Obviously, the neutral efflux through the grid system – and therefore also the propellant flow rate $\dot{V}$, the propellant efficiency, etc. – depend not only on the grids, but also on the gas species. To calculate the neutral gas flow, the gas flow conductivity L_G of a grid has to be defined ($d = grid\ thickness$, $r = hole\ radius$, $T_o = gas\ temp.\ in\ the\ ionizer$, $m_0 = mass\ of\ a\ neutral\ particle$) (23):

$$L_G = \frac{Nr^2}{\frac{3}{8}\frac{d}{r} + 1} \cdot \sqrt{\frac{\pi k T_0}{2 m_0}} \qquad 13$$

In a two- or three-grid-system, the flow resistances $1/L$ are connected serial. Thus, one gets the total grid system conductivity L:

$$\frac{1}{L} = \frac{1}{L_{G1}} + \frac{1}{L_{G2}} + \frac{1}{L_{G3}} \qquad 14$$

Having L and the discharge pressure p_I (see above) the neutral gas-losses $\dot{V}_0$ can be calculated. To compute the total gas flow rate $\dot{V}$ the gas consumption of the ions $\dot{V}_i = 13.93\ SCCM/A \cdot I_i$ and V_0have to be added:

$$\dot{V}_0 = L \cdot p_i \ and\ \dot{V} = \dot{V}_i + \dot{V}_0 \qquad 15$$

I. Basic equations

The RIT-10 should be operated with Xenon (for comparison), Nitrogen, Oxygen, and with a combination of them. Looking at the q_i-curve of Figure 13 and regarding the high dissociation energy $W_{diss} = 9.76\ eV$ of Nitrogen, the portion of N^+ ions should be negligible. As the recombination rate of the collected Oxygen atoms from the atmosphere may be less than 100 % and due to the higher ionization cross sections ofFigure 14, O^+ ions should not be omitted, even if the O_2^+ ions will be dominant.
The performance mapping tests yield the PHV-current I_i, the NHV-current I_{acc} (giving also the beam current $I_{Beam} = I_i - I_{acc}$) as functions of the rf-generator power P_{rf}, the total gas flow rate $\dot{V}$, the positive high voltage U_+, and the negative high voltage U_-.
The mass flow rate $\dot{m}$ can be calculated from the volume flow rate $\dot{V}$ taking the particle mass m into account.
The thrust F of an ion engine is given in general:

$$F = I_{Beam} \cdot \eta_{hom} \cdot \eta_{div} \cdot \sqrt{2 \frac{m_{ion}}{q_{ion}} (U_+ + V_p)} \qquad 16$$

With the typical divergence efficiency $\eta_{div} = 0.98$, homogeneous efficiency $\eta_{hom} = 0.99$ (15) and a mean ion charge $q_i = 1.01\ e$, we get the simplification:

$$F = a \cdot \frac{I_{Beam}}{[A]} \cdot \sqrt{\frac{U_+ + V_P}{[kV]}} \qquad 17$$

With the same beam current and the same voltages, $O_2^+$and N_2^+ generate a thrust that amounts only 0.494 times and 0.462 times of the Xe^+-thrust, respectively.
The power consumption P of the thruster may be written as the sum of all individual contributions:

$$P = I_i U_+ + I_{acc} U_- + P_{rf} = I_i (U_+ + \beta U_- + \omega_i) \qquad 18$$

Note that I_{acc} or $\beta = I_{acc}/I_i$ depends strongly on $\dot{V}$, i.e. the pressure between the grids, because the drain currents is caused mainly by CEX processes. As the ambipolar power losses $P_A \sim 1/\sqrt{m_i}$ (see Equ.7) increase with decreasing ion mass, we may suppose that the ion production costs for O_2 and N_2 are approximately 2.02 times or 2.17 times higher than with Xe (assumed that the other parameters like V_P and n_i are the same).
As usual, we write for the power or electric efficiency:

$$\eta_e = \frac{I_b (U_+ + V_P)}{P} \qquad 19$$

The propellant or mass efficiency is given by (18):

$$\eta_m = \frac{\dot{V}_i}{\dot{V}_i + \dot{V}_0} = \frac{13.93\ SCCM/A \cdot I_b}{\dot{V}} \qquad 20$$

As the gas conductivity of the RIT-engine used for the RAM EP-tests is $L \sim 1/\sqrt{m_0}$ (see Equ. 13), the neutral gas losses of O_2 and N_2 should be 2.02 times and 2.17 times, respectively, higher than those of Xe; thus, the propellant efficiency η_m will be significantly smaller in the case of the atmospheric gases.
This seems to compensate more or less the radical m_i-benefit in the formula of the specific impulse (18):

$$I_{sp} = \frac{1}{g} \cdot \eta_{div} \cdot \eta_m \cdot \sqrt{2 \frac{q_{ion}}{m_{ion}} (U_+ + V_P)} \qquad 21$$

We write again a simplification and include the I_{sp}-coefficient b:

$$I_{sp} = b \cdot \eta_m \cdot \sqrt{\frac{(U_+ + V_P)}{kV}} \qquad 22$$

Note that O_2 and N_2 have a coefficient b being again 2.02 times and 2.17 times greater than the value of Xe.

J. Comparison between the predicted and measured performance values

By using the basic equations of chapter I, the mathematical model yields the RAM-RIT-10 performance data with Xe, N_2, and O_2 while operating the engine with a beam current of 234 mA (Artemis-application).

$I_b = 234\ mA$	Xe	N_2	75 % O_2 + 25 % O
Rf-power P_{rf} $[W]$	102.5 (101.3)	208.5 (207.5)	177.2 (178.2)
Ion production costs w_i $[eV/ion]$	429.6	890	755
Gas flow rate $\dot{V}$ $[SCCM]$	5.0 (5.5)	9.3 (9.9)	8.2 (10.5)
Mass flow rate $\dot{m}$ $[mg/s]$	0.489	0.194	0.170
Discharge pressure p_t $[10^{-4}\ Torr]$	5.86	8.63	6.52
Drain current percentage β [%]	2.1	2.5	1.9
Accel grid drain current I_{acc} $[mA]$	4.9	5.9	4.4
Thrust F $[mN]$	14.71	6.83	6.79
Specific impulse I_{sp} $[s]$	3100	3636	4328
Thruster power input P_{Total} $[W]$	467	574	540
Propellant efficiency η_m [%]	65.2	35.1	39.1
Power efficiency η_e [%]	76.5	63.0	70.3

Table 1: RAM-RIT-10-EBB performance data of Xe, N_2 and O_2 for an ion current of $I_i = 234\ mA$ and voltages of $U_+ = 1500\ V$ and $U_- = -600\ V$; ~25 % Oxygen will be dissociated

The comparison between the measured values (in red) and the theoretical values (in black) show a very good agreement for Xenon and Nitrogen, but for Oxygen a deviation in the gas flow of around 20 % can be seen between the measured value and the predicted value. The reason can be identified in the approximation of the degree of the dissociation. A deviation of ~20 % for the degree of dissociation would results in such a deviation between the calculated gas flow and the measured one.
Therefore it is strongly recommended that tests with gas mixtures should include also a mass spectrometer and a plasma monitor to take care about these facts and to gain further details on the extracted beam while operating the thruster with gas mixtures, especially with different gas types. N_2 and O_2 are quite comparable in this point, except the dissociation aspect.
Beside of the uncertainty in the degree of dissociation, there could be another source of failure due to the uncertainty in the calculation of the flow conductance for atomic oxygen.
The theoretical modeled performance values of the thruster could be validated and show a good agreement with the experimental data. The maximum thrust levels for the RAM-RIT-10 thruster, achievable with 450 W total-power, are summarized in the following table. The table shows the improvement of the thruster performance after the modifications. The orange marked values are based on the measured values before the modifications were implemented.

References

[1]Di Cara, D., et al., "RAM Electric Propulsion for Low Earth Orbit Operation: an ESA study", IEPC-2007-162, 30th International Electric Propulsion Conference, Florence, Italy, Sept. 17-20, 2007.
[2]Rossetti, P., et al." Preliminary characterization test of HET and RIT with Nitrogen and Oxygen", AIAA-2011-6073, 47th AIAA/ASME/SAE/ASEE Joint Propulsion Conference and Exhibit, San Diego, California, July 31-3, 2011.

[3]Feili, D. et al., "Testing of new μN-RITs at Giessen", 41st AIAA/ASME/SAE/ASEE Joint Propulsion Conference & Exhibit 10 - 13 July 2005, Tucson, Arizona